International Journal of GEOMATE, May, 2025 Vol.28, Issue 129, pp.97-104
ISSN: 2186-2982 (P), 2186-2990 (O), Japan, DOI: https://doi.org/10.21660/2025.129.g14045
Geotechnique, Construction Materials and Environment

EFFECTS OF HETEROGENEOUS SPATIAL PERMEABILITY OF RIVER EMBANKMENTS ON SEEPAGE BEHAVIOR

*Hideaki Yoshida[1], Koji Nakashima[2], and Katsuyuki Kawai[2]

[1]Graduate School of Science and Engineering, Kindai University, Japan; [2]Faculty of Science and Engineering, Kindai University, Japan

*Corresponding Author, Received: 02 Jan. 2025, Revised: 04 Feb. 2025, Accepted: 12 Feb. 2025

ABSTRACT: The number of levee breaches caused by intense rainfall and typhoons is increasing in Japan, and the potential for extensive damage is growing. To minimize damage, it is essential to prevent levee breaches or, at least, to lengthen the time leading up to failure. One of the causes leading to failure is reduced stability and deterioration of the embankment due to internal erosion. Previous studies have implicated changes in the strength and stability of embankment soils due to internal erosion. However, the relationship between permeability changes due to seepage and stability is not yet clear. This study conducted seepage tests on an embankment model simulating a river embankment to evaluate the effects of various seepage histories on changes in the hydraulic conductivity and grain size distribution of the embankment. In addition, seepage analyses were carried out assuming spatial variation in hydraulic conductivity due to internal erosion, and the effects on seepage behavior were evaluated. Results confirmed that seepage causes the migration of fine grains, leading to heterogeneous permeability. Furthermore, repeated seepage intensified the fine particle movement within the embankment and reduced the hydraulic conductivity. It was also found that the phreatic surface within the embankment became higher when the permeability of the backslope decreased, whereby the local hydraulic gradient increased. In addition, the results confirmed that the analytical model in this study can express seepage behavior and instability of river embankments over time.

Keywords: Internal erosion, Seepage, River embankment, Deterioration, Model simulating

1. INTRODUCTION

Short-time intense rainfalls and torrential rainfalls exceeding 1,000 mm total have frequently occurred in Japan. This trend has resulted in many levee breaches throughout Japan. In 2019, typhoons caused levee breaches over a wide area, with the Chikuma River levee breach causing the most serious damage [1-3].

While overtopping is the main cause of many of the breaches, damage to the levees, such as the collapse of back slopes due to seepage, also leads to the breaches. River levees are long-span and have heterogeneous soil characteristics. Therefore, the soil characteristics often differ between the failure areas and the remaining areas. Post surveys are mainly conducted on the remaining areas that did not fail, whereby it is difficult to determine the causes of failure. There is a possibility of errors occurring when identifying the cause of the breach.

One of the causes of the weakening of levees against seepage is the deterioration of the soils due to internal erosion. Internal erosion is the migration of fine particles in the ground due to seepage, such as water table fluctuations and rainfall, which affects the instability of levees. Several experiments and analyses to clarify the effects of internal erosion on the instability of soils have previously been conducted. Johnston et al. [4] investigated the effects of fine-grain migration on the permeability, shear wave velocity, stiffness, and strength of embankment materials. Rupali et al. [5] focused on the phenomenon of suffusion of fine-grained pumice sand and showed that physical properties such as hydraulic conductivity and shear strength are affected by suffusion. Sanjei et al. [6] studied the effect of seepage flow on the liquefaction resistance of coarse-grained soils and reported that seepage flow causes the rearrangement of coarse particles and reduces liquefaction resistance. Nakashima et al. [7] evaluated the effect of material properties and seepage conditions on heterogeneity due to internal erosion and reported that the effect of relative density on the occurrence of internal erosion is significant. Although these studies partially elucidated the mechanism of internal erosion and its effects, the mechanical behavior of the embankment caused by changes in soil properties due to seepage and the relationship to the stability of the overall embankment. In addition, there is a lack of knowledge on the mechanical stability of the embankment when seepage conditions such as rainfall and river water table fluctuations act simultaneously. In addition, few studies have systematically evaluated the effects of these combined seepage conditions on the development of internal erosion.

In this study, to evaluate the effects of different seepage histories on the changes in hydraulic conductivity and grain size distribution of the levee component soil, permeability tests on a levee model

simulating a river levee were performed. In addition, seepage analysis simulating spatial changes in hydraulic conductivity due to internal erosion was conducted to evaluate the effects on the seepage behavior.

2. RESEARCH SIGNIFICANCE

In the current inspection of river embankments, seepage and piping are routinely verified; however, internal erosion is not adequately considered. With the anticipated increase in intense rainfall events in the future, river levees are expected to be continuously subjected to seepage, which may lead to progressive weakening due to internal erosion. Therefore, it is critical to incorporate internal erosion into the evaluation process. This study aims to clarify the effects of internal erosion under combined seepage conditions such as simultaneous rainfall and fluctuating river water levels and to obtain the necessary knowledge that can be applied to enhance maintenance and management practices for river embankments.

3. OUTLINE OF THE MODEL EXPERIMENT

3.1 Experimental Apparatus

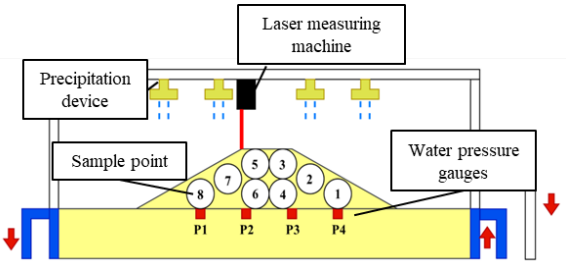

Fig. 1 Outline of the experimental apparatus

Table 1. Soil properties of test material

Maximum density	ρ_{dmin} (g/cm^3)	1.366
Minimum density	ρ_{dmax} (g/ cm^3)	1.782
Maximum void ratio	e_{min}	0.734
Minimum void ratio	e_{max}	1.017
Density of soil particles	ρ_s (g/ cm^3)	2.749
Hydraulic conductivity	k (cm/s)	1.54E-03

Fig. 1 shows an overview of the embankment model and the measurement apparatus used in the experiment. A 110 mm high model embankment with a base of 100 mm and a slope of 1:2 was prepared in an acrylic soil tank with internal dimensions of 900 mm x 500 mm x 300 mm. After the experiment, samples were taken from locations 1~8 shown as in Fig.1, and constant head permeability tests and grain size analysis were then conducted on the sampled soil. A total of four water pressure gauges were installed in the embankment model between the foundation and the embankment to confirm water table fluctuation due to seepage, and a laser displacement meter was installed on top of the model to measure the deformation of the embankment. In addition, a camera was installed on top of the embankment model to observe changes in the embankment over time.

3.2 Experimental Conditions

As the test material, decomposed granite soils were used with a grain size distribution shown in Fig. 2. To confirm the effect of internal erosion, test material which has the potential to have internal instability based on the internal stability index [8]. To assess the physical properties of the test material, several fundamental tests were conducted, including maximum and minimum density tests, density tests of soil particles, and permeability tests. The results of these tests are summarized in Table 1.

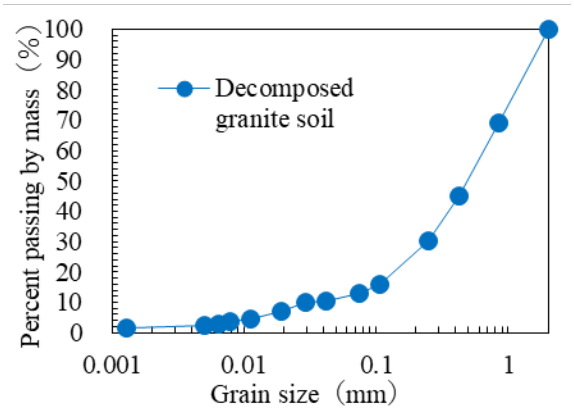

Fig. 2 Grain size distribution of decomposed granite soil

Table 2. Model test conditions

Case1	Water table rising	90% of the embankment height
Case2	Rainfall	65mm/hr
Case3	Water table rising and rainfall	90% of the embankment height + 65mm/hr
Case4	Repeated water table rising	90% of the embankment height ⇔ Foundation level

The method for preparing the embankment model is as follows. First, based on the results of the physical property tests, the test materials were prepared. Next, distilled water was added to reach a water content

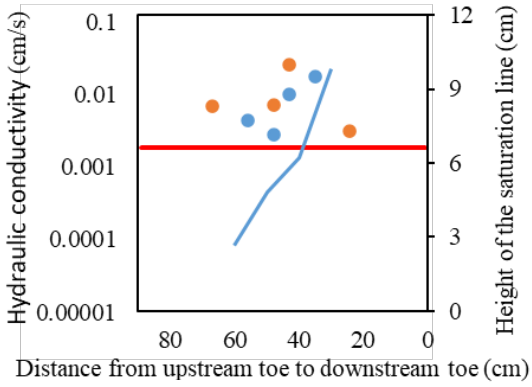

(a) Case1

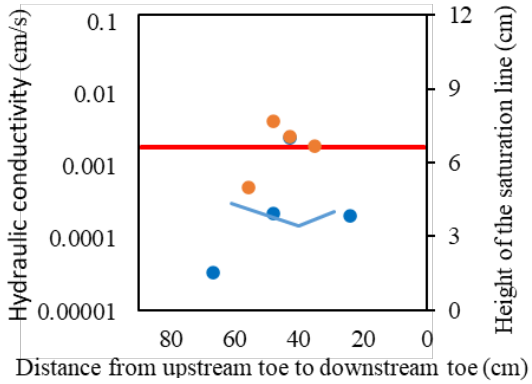

(b) Case2

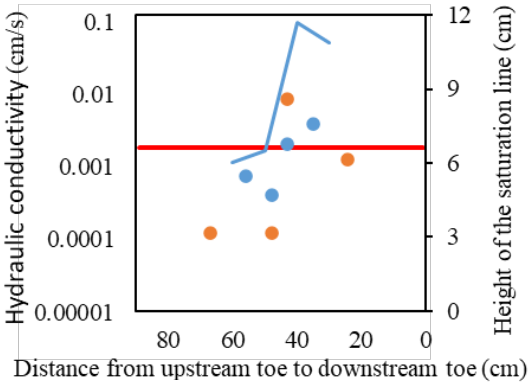

(c) Case3

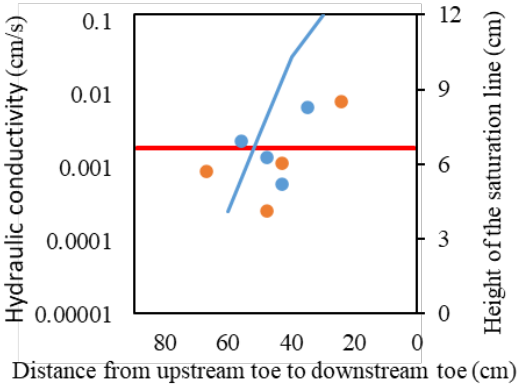

(d) Case4

Fig. 3 Seepage test results

ratio of 10% and mixed so that it was evenly distributed. After that, each layer of the prepared soil mixture was placed in a soil tank and compacted into 5cm (6 cm for the top layer) with a relative density of 60%, this process was repeated for all four layers. Finally, the slope was cut to a ratio of 1:2, leaving a crest width of 100 mm.

The seepage conditions (Cases) for the model experiments are shown in Table 2. In Case 1, the water table was 90% of the outside water table, and in Case 2, water was sprayed at a rate of 65 mm/hr to simulate intense rainfall. In Case 3, conditions from cases 1 and 2 were applied simultaneously. In Case 4, a water table of 90% of the outside water table was applied for 1 hour, and then the water table was lowered to the foundation level and retained for 1 hour. This condition was applied a total of three times, assuming age deterioration due to repeated seepage history. In each case, the soil was allowed to infiltrate for a total of 6 hours. The water table was set at 10 cm for 12 hours to saturate the foundation soil before the experiment.

In Cases 2 and 3, the permeability was less than the intense rainfall, and surface flow occurred. However, no shape changes or soil erosion of the embankment due to surface flow was observed. Therefore, the occurrence of surface flow is not considered to be a problem for the stability of the embankment.

4. RESULTS AND DISCUSSION OF MODEL TESTS

4.1 Hydraulic Conductivity

The results of the seepage test are shown in Fig. 3. The upper section (orange dots) and lower section (blue dots) of the embankment are shown in the figure, along with the phreatic surface after one hour (blue line) and the hydraulic conductivity before the experiment started (red line). From the experimental results, Case 1 shows that the overall hydraulic conductivity increased compared to the pre-experiment values. In contrast, Case 2 shows that the hydraulic conductivity significantly decreased in parts of the upper and lower sections compared to the pre-experiment values, while other areas remained almost the same. In Case 3, the hydraulic conductivity increased on the upstream side and decreased on the downstream side of the model compared to the pre-experiment values; while in Case 4, some parts of the upstream side saw an increase in the hydraulic conductivity, with other areas experiencing a decrease.

To consider the impact of different seepage conditions and repeated seepage histories on the hydraulic conductivity, Cases 1 through Case 4 were compared. Comparing Case 1 and Case 2, significant

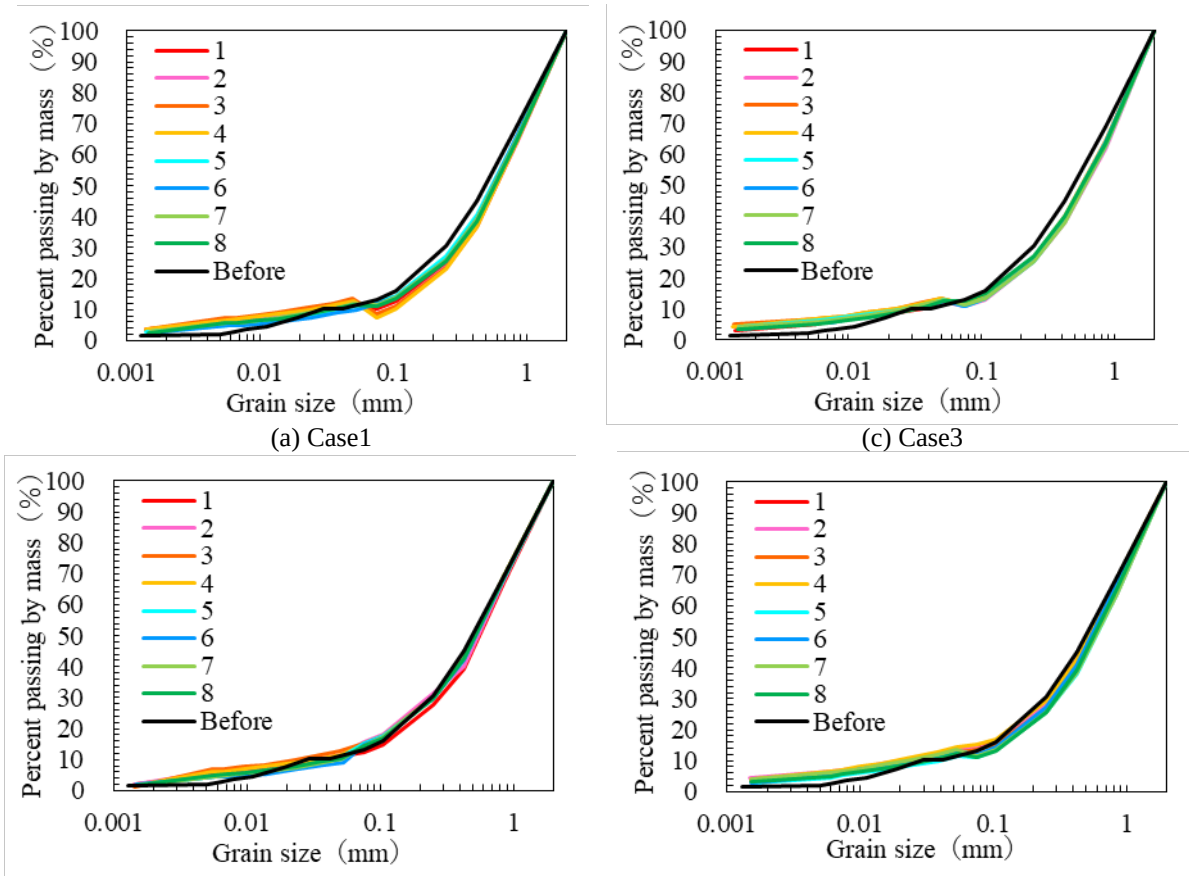

(a) Case1 (c) Case3

(b) Case2 (d) Case4

Fig. 4 Grain size distribution results

differences in the hydraulic conductivity changes were noted between the upstream and downstream sides of the model during river flooding and between the upper and lower sections during rainfall, which is thought to be due to the movement of fine particles according to the magnitude and direction of seepage. Next, when comparing Cases 1, 2, and 3, the hydraulic conductivity increased on the upstream side of Case 3 due to fine particle movement towards the middle of the embankment caused by seepage; and it decreased on the downstream side due to particle movement towards the lower side of the slope caused by rainfall seepage. This suggests that simultaneous flooding and rainfall could result in hydraulic conductivity changes exhibiting characteristics of seepage. Finally, when comparing Cases 1 and 4, Case 4 showed a more significant overall decrease in hydraulic conductivity than the pre-experiment values, with greater spatial variability. This indicates that repeated seepage decreases the hydraulic conductivity gradually, suggesting that repeated seepage histories cause more significant changes in the hydraulic conductivity than a single event.

4.2 Grain Size Distribution

The results of the grain size analysis are shown in Fig. 4. In Case 1, coarse particles decreased overall, while fine particles increased. For Case 2, excluding sample 1, the distribution of coarse particles was like the pre-experiment distribution, and fine particles increased in all areas. In Case 3, coarse particles decreased overall, and fine particles increased. In Case 4, coarse particles decreased on the downstream side, and fine particles increased.

By comparing Cases 1 through 4, the impact of different seepage conditions and repeated seepage histories on the grain size distribution can be considered. First, comparing Case 1 and Case 2 by sampling locations shows that in Case 1, the decrease in coarse particles and the increase in fine particles was greater on the upstream side (positions 1 to 4). Conversely, on the downstream side (positions 5 to 8), the decrease in coarse particles was smaller, and the increase in fine particles was also smaller. In Case 2, the change in coarse particles was minimal overall, and the increase in fine particles was smaller than in Case 1. This indicates that seepage due to river flooding has sufficient force to move coarse particles, whereas rainfall seepage does not have the force to move coarse particles but does have the force to move fine particles. However, in actual river levees, the amount of rainfall seepage into the embankment is small, and thus the force needed to move soil particles

is weak, making it unlikely that fine particles would flow to the lower part of the embankment. Therefore, the results of this experiment are likely related to the dimensions of the model. Next, in comparing Cases 1, 2, and 3, fine particles moved to the center of the embankment on the upstream side due to the flood as shown in Case 3. In this case, as the phreatic surface was fully formed due to the flood, the impact of rainfall was minimal. On the other hand, on the downstream side of Case 3, the impact of flooding was minimal, and fine particles moved from the upper to the lower part of the embankment due to rainfall seepage.

Finally, in comparing Cases 1 and 4, fine particles in Case 1 moved to the center of the embankment, while fine particles in Case 4 moved further to the downstream side due to repeated seepage. These results demonstrate that with repeated seepage, fine particles that only moved to the center of the embankment in a single event moved to the downstream side with repeated events.

4.3 Discussion

The results of the hydraulic conductivity and grain size distribution analyses found that the increase in fine particles due to seepage decreased the hydraulic conductivity. Moreover, repeated seepage histories intensified the migration of fine particles, whereby the hydraulic conductivity decreased. Therefore, it is suggested that repeated seepage conditions are more likely to cause internal erosion.

5. SEEPAGE ANALYSIS CONSIDERING SPATIAL DISTRIBUTION OF PERMEABILITY

In the model experiment, it was found that the distribution of the hydraulic conductivity within the embankment changes due to internal erosion during seepage. Here, through numerical simulations, the influence of the hydraulic conductivity distribution on seepage behavior within the river embankment is investigated.

5.1 Mathematical Models

In this study, soil/water/air-coupled finite element analysis code, DACSAR-MP [9], is used. This analysis code can consistently express the flow of both water and air with the deformation of the ground. The mechanical models used there are as follows. The constitutive model for unsaturated soil is given by the following equation.

$$\boldsymbol{\sigma}' = \mathbf{D} : \boldsymbol{\varepsilon} - \mathbf{C} \cdot \dot{S}_e \tag{1}$$

Here, $\boldsymbol{\sigma}'$ is the effective stress tensor for unsaturated soil, is the elastoplastic stiffness matrix, $\boldsymbol{\varepsilon}$ is the strain tensor, $\mathbf{C}$ is the tensor that expresses the change in stiffness due to desaturation, and is the effective degree of saturation. The effective stress for unsaturated soil is expressed by the following equation.

$$\boldsymbol{\sigma}' = \boldsymbol{\sigma}^{net} + p_s \mathbf{1} \tag{2a}$$

$$\boldsymbol{\sigma}^{net} = \boldsymbol{\sigma} - p_a \mathbf{1}, \;\; p_s = S_e s \tag{2b}$$

$$s = p_a - p_w, \;\; S_e = \frac{S_r - S_{rc}}{1 - S_{rc}} \tag{2c}$$

Here, $\boldsymbol{\sigma}^{net}$ is the net stress tensor, $\mathbf{1}$ is the unit tensor, $\boldsymbol{\sigma}$ is the total stress tensor, s is suction, p_s is the suction stress, p_a is pore air pressure, p_w is pore water pressure, S_r is the degree of saturation, and is the asymptotic degree of saturation at $s \to \infty$. The continuity equations for pore water and pore air are given by equations (3) and (4), respectively.

$$n\dot{S}_r - S_r \dot{\varepsilon}_v + \mathrm{div}\tilde{\mathbf{v}}_\mathbf{w} = 0 \tag{3}$$

$$\left(1 - S_r\right)\dot{\varepsilon}_v + n\dot{S}_r - n\left(1 - S_r\right)\frac{\dot{p}_a}{p_a + p_0} - \mathrm{div}\tilde{\mathbf{v}}_\mathbf{a} = 0 \tag{4}$$

Here, n is the porosity, $\tilde{\mathbf{v}}_\mathbf{w}$ and $\tilde{\mathbf{v}}_\mathbf{a}$ is the relative velocity vector for pore water and pore air respectively, ε_v is the volumetric strain, and p_0 is the atmospheric pressure. The models proposed by Mualem [10] and van Genuchten [11] are used for the unsaturated permeability of water and air, respectively.

$$k_{rw} = S_e^{1/2}\left[1 - \left(1 - S_e^{1/m}\right)^m\right]^2 \tag{5}$$

$$k_{ra} = \left(1 - S_e\right)^{1/2}\left(1 - S_e^{1/m}\right)^{2m} \tag{6}$$

Here, k_{rw} , k_{rw} are the specific hydraulic conductivity for pore water and pore air, respectively, and m is a shaping parameter. The water retention characteristic curve, which represents the relationship between soil moisture and suction, is known to differ between drying and wetting processes and to depend on the suction history. In this study, the water retention curve model proposed by Kawai et al., which accounts for the effects of hysteresis, is adapted. The constitutive model and continuity equations are coupled through the effective stress and the water retention curve model, enabling the simultaneous representation of deformation and seepage behaviors.

5.2 Simulation Conditions

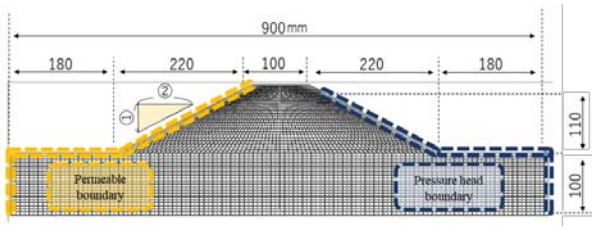

(a)Case1

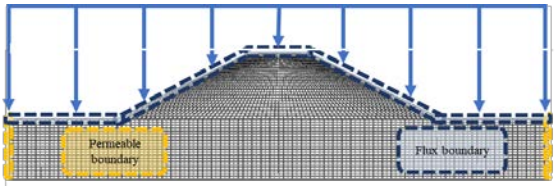

(b)Case2

Fig. 5 Analytical meshes and boundary conditions

Fig. 6 shows the analytical meshes and boundary conditions to simulate the model experiment. Case 1 was prepared as a river water table rise test, and Case 2 as a rainfall test. The river water table rise was expressed by applying a pressure head equivalent to the water table to the embankment slope (indicated by the blue line in Fig. 5 (a)). Rainfall was applied as a flux boundary condition equivalent to the rainfall intensity on the crest, slope, and riverbed (indicated by the blue line in Fig. 5 (b)). Here, the flux applied to the slope was reduced to account for the gradient. The orange lines in the figure represent permeable boundaries. The permeable boundary is a hybrid boundary where it acts as an impermeable boundary when the pressure head is negative but transitions to a zero-pressure head condition when the pressure head becomes positive.

The input parameters used for simulations are summarized in Table 3 and the water retention characteristics curve is shown in Fig. 6. The hydraulic conductivity in Table 3 was set as the reference case (Cases 1-1 and 2-1), and additional analysis cases were prepared to account for changes in the hydraulic conductivity distribution due to internal erosion. As observed in the model experiments, changes in the hydraulic conductivity are particularly pronounced around the slope toe. There, in Cases 1-2 and 2-2, the hydraulic conductivity within the area enclosed by the red lines in Fig. 7 was reduced to one-hundredth. This simulation condition represents the accumulation of fine particles, transported by seepage within the river embankment, around the slope toe, leading to a reduction in the hydraulic conductivity. Meanwhile, in Cases 1-3 and 2-3, the hydraulic conductivity was increased by a factor of 100. This simulation condition represents the outflow of transported fine particles from the river embankment, resulting in an increase in hydraulic conductivity. The simulation procedure is as follows. First, an initial condition of

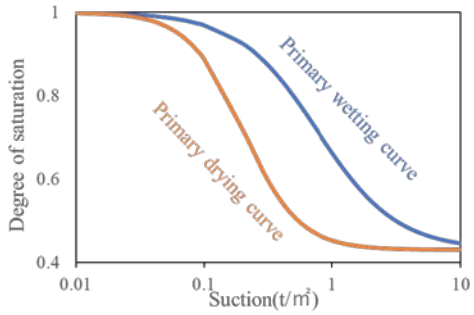

Fig. 6 Water retention characteristics curves

Table 3. Input material properties

λ	κ	M	k_{wx}	k_{wy}
0.087	0.009	1.375	1.8	0.9
m	a	n_s	k_{ax}	k_{ay}
0.6	10.0	1.0	180	90

0.9 saturation and a pressure head of -0.15m is assigned to all nodes, followed by 1 1-day resting period. Subsequently, in Case 1, a pressure head was applied up to 90% of the crest height on the right slope, as shown in Fig 5, and on the riverbed and left as it was for 6 hours. In Case 2, a rainfall intensity of 6.5 mm/h was applied to the top surface of the analysis domain for 1 hour.

5.3 Simulation Results

The results obtained from simulations representing the rise in river level are shown in Fig. 8. These are the conditions at the completion of the simulation. The color contours represent the pressure head distribution, and the solid black lines represent a group of equipotential lines. In the figure, the position where the pressure head is zero is indicated as the phreatic surface, shown with a light blue broken line. Cases 1-1 represent the conditions in the model experiment where the hydraulic conductivity of the material prior to seepage was uniformly applied throughout. Here, a downward-inclining phreatic surface from the river water table toward the landside slope was observed. From the equipotential lines, it was evident that the flow velocity gradually decreased as it moved toward the landside. Case 1-2 represents the condition where clogging due to fine particle migration occurred at the slope toe, resulting in a decrease in hydraulic conductivity. Compared to Case 1-1, the phreatic surface around the slope toe rises, and the spacing between the equipotential lines also becomes narrower. An increase in the hydraulic gradient at the slope toe decreases the stability of the embankment, indicating a transition to a hazardous condition for the river embankment. When the water pressure increases at the slope toe, the effective stress decreases, which may cause localized failure. This

(a) Case 1 (b) Case 2

Fig. 7 Locations where the hydraulic conductivity was modified

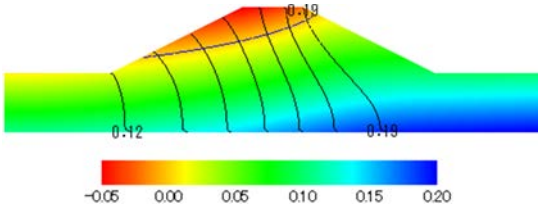

(a) Case1-2

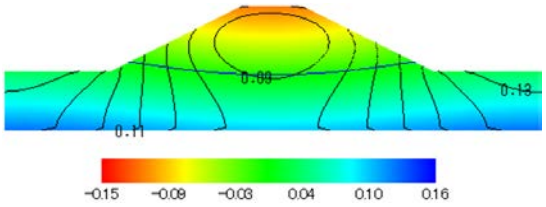

(b) Case2-1

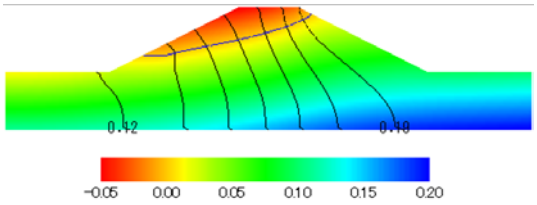

(b) Case1-2

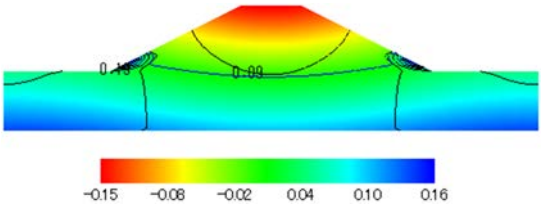

(b) Case2-2

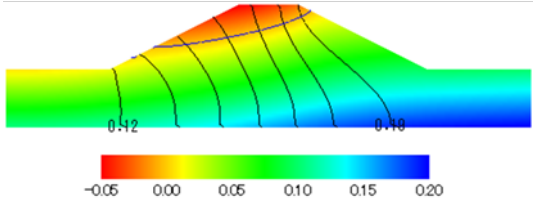

(c) Case1-3

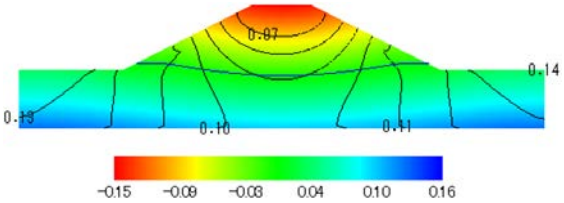

(c) Case2-3

Fig. 8 Water table rising simulation

Fig. 9 Rainfall simulation

type of localized failure in the flow direction is called piping failure. When piping failure occurs, the failure area gradually expands upstream, and during this process, an area with a higher hydraulic conductivity may develop around the slope toe like in Case 1-3. In Cases 1-3, the phreatic surface around the slope toe is lower, and the spacing between the equipotential lines is wider.

The results obtained from rainfall simulations are shown in Fig. 9. In all cases, from the color contours, it can be observed that the central part of the embankment exhibits a smaller pressure head compared to the edges on either side, indicating that the pressure head distribution is still in an unsteady state and has not yet reached a hydrostatic pressure distribution. The phreatic surface is also convex downward in the central part. From the equipotential lines, it can be observed that around the slope surface of the embankment, the flow is parallel to the slope and directed toward the slope toe. In Case 2-2, where the hydraulic conductivity around the slope toe is small, the hydraulic gradient at the slope toe is large (indicated by the narrow spacing between the equipotential lines), whereas in Case 2-3, the opposite distribution is observed.

6. CONCLUSIONS

In this study, model tests simulating a river embankment were conducted to investigate the effects of different seepage conditions, such as river level rise and rainfall, on the grain size distribution within the embankment. In addition, a seepage analysis was conducted to evaluate the effect of changes in permeability distribution due to internal erosion on the mechanical stability of the embankment. The conclusions obtained from this study and future issues are as follows.

(1) The results of the model test indicated changes in the hydraulic conductivity distribution, suggesting alterations in the grain size

distribution after seepage. After seepage simulation river level rises, and the hydraulic conductivity tends to decrease from the riverside to the landside due to the water table rising. On the other hand, on the model test simulating rainfall, although no significant differences were observed, there was a slight tendency for the hydraulic conductivity to decrease toward the slope toe. These results are thought to indicate the effects of internal erosion, where fine particles migrate from the inflow side to the outflow side, causing clogging and reducing the hydraulic conductivity. Changes in grain size distribution showed migration of fine grains by seepage in both water table rising and rainfall, and the amount of migration varied depending on the intensity of seepage.

(2) The effects of changes in hydraulic conductivity distribution due to internal erosion were investigated through numerical simulations. Since the discharge area of the infiltrated water from the embankment is at the slope toe, the change in hydraulic conductivity at the slope toe was taken into account. Consequently, the decrease in hydraulic conductivity due to clogging at the slope toe as a discharge area was found to increase the hydraulic gradient locally around the slope toe. This, in turn, reduces the stability of the embankment and increases the risk of failure. These results support the fact that the rearrangement of soil particles results in lower permeability as they are repeatedly varied, as pointed out in previous studies [12].

Since embankments are exposed not only to simple river water table rises or rainfall but also to a combination of external forces over time, long-term river embankment management requires investigating detailed behavioral changes through model experiments with varying seepage conditions.

7. ACKNOWLEDGMENTS

This work was supported by Grant-in-Aid for Scientific Research (21K14244).

8. REFERENCES

[1] Cabinet office government of Japan, Damage from Typhoon No.19 in 2018. 2020, pp. 24-27 (in Japanese).

[2] Ohtsuka S., Sato Y., Yoshikawa T., Sugii T., Kodaka T., Maeda K., Levee damage and revetment erosion by the 2019 Typhoon Hagibis in the Chikuma River. Soils and Foundations, Vol. 61, No. 4, 2021, pp. 1172-1188.

[3] Matsuda T., Kawajiri S., Watanabe Y., Watanabe K., Investigation of river structures damaged at Chikuma River due to typhoon No. 19, October 2019. JSCE, Vol. 10, No. 1, pp. 206-212.

[4] Johnston I., Murphy W., Holden J., The effects of internal erosion on granular soils used in transport embankments. Soils and Foundations, Vol. 64, Issue 1, 2024, 101424.

[5] Rupali S., Watabe Y., Suffusion in densely compacted Satozuka pumice sand and its impact on static loading undrained shear strength and dilation behaviour. Soils and Foundations, Vol. 63, Issue 6, 2023, 101397.

[6] Sanjei C., Otsubo M., Kuwano R., Effects of seepage flow on liquefaction resistance of uniform sand and gap-graded soil under undrained cyclic torsional shear. Soils and Foundations, Vol. 63, Issue 5, 2023, 101363.

[7] Nakashima K., Kawai K. and Fumoto T., Impacts of suffusion factor on heterogenization of soils. International Journal of GEOMATE, Vol. 21, Issue 88, 2021, pp.22-27.

[8] Kenney T. and Lau D., Internal stability of granular filters. Canadian Geotechnical Journal, Vol. 22, No. 2, 1985, pp. 215-225.

[9] Sugiyama Y., Kawai K., Iizuka A., Effects of Stress Condition on B-value Measurement. Soils and Foundation, Vol. 56, No. 5, 2016, pp. 848-860.

[10] Mualem Y., A New Model for Predicting the Hydraulic Conductivity of Unsaturated Porous Media. Water Resources Research, Vol. 12, No. 3, 1976, pp. 514-522.

[11] van Genuchten., A Closed-form Equation for Predicting Hydraulic of Unsaturated Soils. Soil Science Society American Journal, Vol. 44, 1980, pp. 892-898.

[12] Sato M., Kuwano R., One-dimensional seepage test studying factors for internal erosion. Industrial Science, Vol. 66, No. 4, 2014, pp. 331-335. (in Japanese).